communications chemistry

A Nature Portfolio journal

Article

https://doi.org/10.1038/s42004-025-01522-1

Semi-synthesis of TDP-43 reveals the effects of phosphorylation in N-terminal domain on self-association

Daisuke Sasaki ✉, Mao Tenda & Youhei Sohma ✉

TDP-43, a nucleocytoplasmic shuttle protein consisting of 414 residues, forms self-association in the nucleus for physiological gene regulation, while aggregation into amyloid (consisting of aberrant β-sheets) in the cytoplasm causes neurodegenerative diseases such as amyotrophic lateral sclerosis. Post-translational phosphorylation of TDP-43 alters the self-association properties, which affects both the physiological function in the nucleus and the amyloidogenic potential in the cytoplasm, thereby impacting upon disease progression. However, insight into the role of per-residue phosphorylation in the self-association remains limited due to the difficulty in obtaining site-specifically phosphorylated TDP-43. Here, we demonstrate semi-synthesis of full-length TDP-43 that is uniformly phosphorylated at the 48th serine residue (designated as $TDP_{1\text{-}414}$[pS48]). The synthetic scheme consisting of native chemical ligation followed by His-tag affinity chromatography efficiently gave $TDP_{1\text{-}414}$(pS48) with a high purity. Interestingly, unlike non-phosphorylated TDP-43, the phosphorylated TDP-43 was found to have weak self-association property and to form aggregates that were not typical amyloid fibrils. Furthermore, chemical synthesis and three-dimensional structure analysis of the N-terminal domain (NTD, corresponding to $TDP_{1\text{-}80}$) suggested that the phosphate ion at Ser48 weakens the inter-NTD interaction by inducing electrostatic repulsion. It significantly advances understanding of the pathological mechanisms involved in the post-translational modifications of TDP-43 associated with the neurodegenerative diseases.

Transactive response DNA-binding protein 43 kDa (TDP-43)[1], is a 414 amino acid protein that consists of an N-terminal domain (NTD), two RNA recognition motifs (RRM1 and RRM2), and a C-terminal low-complexity domain (LCD), and it shuttles between the nucleus and cytoplasm (Fig. S1)[2]. TDP-43 forms self-association in the nucleus to play indispensable roles in RNA metabolism[3]. Conversely, TDP-43 exported from the nucleus to the cytoplasm can undergo aggregation to form amyloids consisting of aberrant β-sheets, which causes neurodegenerative diseases such as amyotrophic lateral sclerosis (ALS) and frontotemporal dementia (FTD)[4–6]. Post-translational phosphorylation as well as ALS-linked amino acid mutations of TDP-43 alter the self-association properties, which potentially affect both the RNA metabolism in the nucleus and the amyloidogenic potential in the cytoplasm, thereby impacting the disease progression[7–10]. However, insight into the role of per-residue phosphorylation in the self-association remains limited due to the difficulty in obtaining site-specifically phosphorylated TDP-43.

Chemical synthesis, which offers uniformly-modified protein molecules at specific sites, is a powerful method for investigating the functions of the unique post-translational modifications made to the proteins[11]. Indeed, the pathological properties of the post-translational modifications of tau, α-synuclein, and huntingtin, which cause neurodegenerative diseases by forming amyloids, have been unveiled through semi-synthesis of the uniquely modified respective proteins[12]. Regarding TDP-43, the semi-synthesis approach has focused upon a C-terminal region ranging from around 260 to 414, which corresponds to intrinsically disordered LCD (Fig. 1a). Li et al. semi-synthesized a Ser404-phosphorylated LCD and demonstrated that ALS-associated phosphorylation at the site accelerated amyloid aggregation and induced cytotoxicity[13]. Although not a precedent for post-translational modification, the semi-synthesis of various LCD derivatives with a site-specific methyl-cap on the nitrogen atom of the peptide backbone has been reported, highlighting the importance of main-chain hydrogen bonds for the self-association and phase separation[14]. Conversely, there has been no

Department of Medicinal Chemistry, School of Pharmaceutical Sciences, Wakayama Medical University, Wakayama, Japan.
✉e-mail: dsasaki@wakayama-med.ac.jp; ysohma@wakayama-med.ac.jp

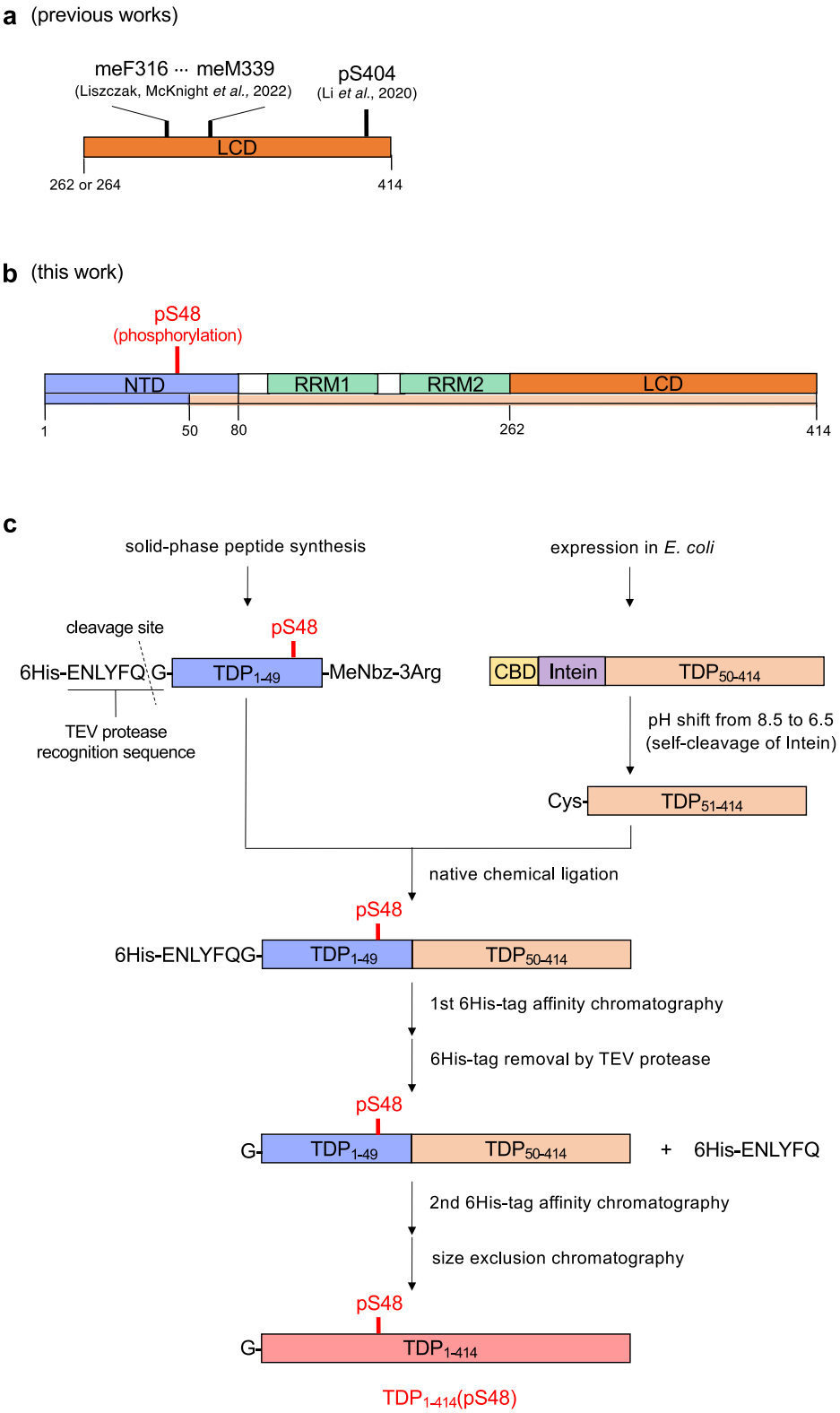

Fig. 1 | Semi-synthesis of TDP-43. a Previously reported C-terminal LCD-modified TDP-43 fragments. me: *N*-methylated peptide bond; pS: phosphorylated Ser. **b** Full-length TDP-43 possessing pS48 (designated as $TDP_{1\text{-}414}$[pS48]) synthesized in this work. **c** Synthetic scheme of $TDP_{1\text{-}414}$(pS48). MeNbz (*N*-acyl-*N*′-methyl-benzimidazolinone) is an *N*-acylurea linker that functions as a thioester surrogate[21]. CBD: chitin-binding domain.

semi-synthesis of NTD-modified TDP-43. Here, we report semi-synthesis of full-length TDP-43 with a phosphorylation on Ser48 (designated as $TDP_{1\text{-}414}$[pS48], Fig. 1b). $TDP_{1\text{-}414}$(pS48) is a rare form that has post-translational modification in the NTD (most ALS-associated modifications are found in the C-terminal LCD), and the functions of $TDP_{1\text{-}414}$(pS48) have attracted interest[3,15]. Wang et al. reported that $TDP_{1\text{-}414}$ in which Ser48 was replaced with Glu as a phosphoserine mimetic had reduced self-association property compared with intact $TDP_{1\text{-}414}$[3]. An intriguing result unveiled by the chemically synthesized $TDP_{1\text{-}414}$(pS48) was that the authentic phosphoserine at position 48 actually attenuates the self-association and confers aggregates that were not typical amyloid fibrils. In addition, three-dimensional structure analysis focusing on NTD suggested that the phosphate ion at Ser48 weakens the inter-NTD interaction by inducing electrostatic repulsion.

Results and discussion

Semi-synthesis of full-length TDP-43

We planned to synthesize TDP_{1-414}(pS48) by reacting TDP_{50-414}, which contains Cys at the N-terminus, with the TDP_{1-49}-thioester by native chemical ligation, which connects two peptide fragments into a protein via chemo-selective thioester exchange with N-terminal Cys followed by an intramolecular acyl transfer (Fig. 1c)[16]. The Cys residue of TDP_{1-414} closest to the C-terminus of Ser48 was selected as the disconnection site of the ligation. The recombinant synthesis of TDP_{50-414} was investigated first. We used a protein purification system, which employed chitin-binding domain (CBD) affinity chromatography combined with a pH-dependent self-cleavable intein element[17]. A construct of CBD-Intein-TDP_{50-414} was expressed in *E. coli*. The protein construct was found to be expressed as an inclusion body (Fig. S2a), so we used the solubilization buffer containing a denaturation reagent, guanidine hydrochloride (Gn-HCl) at 4 M. In addition, the inclusion of a non-ionic detergent, Triton X-100 (final concentration: 2%) in the solubilization buffer was important to prevent protein precipitation during the subsequent dialysis (Fig. S2b). Dialysis, which removes the Gn-HCl, allowed the refolding of the CBD of the construct, gaining the ability to bind to the chitin resin. Thus, after immobilizing the construct to the chitin resin, followed by washing the construct-resin, the pH of the solution was changed from 8.5 to 6.5 to induce the self-cleavage of intein, producing TDP_{50-414} with the N-terminal Cys (Figs. 1c and S2c, d). The Cys-TDP_{51-414} eluted from the resin was sufficiently pure (Fig. S2e) and was isolated as a dried pellet through precipitation with chloroform-methanol mixed solvent. The yield of TDP_{50-414} was 50 mg from 6 L of *E. coli* culture medium. Although isolating a sufficient amount of CTD is generally difficult due to the high aggregation propensity[18], we were able to obtain TDP_{50-414} with high efficiency, presumably because it is accompanied by stably folded and soluble RRM1[19] and RRM2[20] at the N-terminus of CTD, as well as the use of Triton X-100 during the purification.

In preliminary synthetic studies of non-phosphorylated TDP_{1-414}, it was difficult to separate the desired product after the ligation from the remaining starting material Cys-TDP_{51-414} using size exclusion chromatography (Fig. S3). We therefore planned a scheme consisting of native chemical ligation followed by His-tag affinity chromatography for the synthesis of TDP_{1-414}(pS48) (Fig. 1c). First, we confirmed in a model study that the native chemical ligation followed by His-tag affinity chromatography scheme works (Fig. S4). Then, TDP_{1-49}(pS48) attached to a 6× histidine (6His)-tag at the N-terminus via a TEV protease cleavage peptide (TEV: tobacco etch virus; cleavage site by TEV protease is underlined in the following statement) was employed. The N-terminal peptide for the ligation, 6His-ENLYFQG-TDP_{1-49}(pS48)-MeNbz-3Arg, in which *N*-acylurea Nbz linker was adopted as a thioester surrogate (MeNbz: *N*-acyl-*N*′-methylbenzimidazolinone)[21], was synthesized using microwave-assisted Fmoc-based solid-phase peptide synthesis (Fig. S5a). The native chemical ligation was performed with 4 mM N-terminal TDP_{1-49}(pS48) derivative and 0.4 mM Cys-TDP_{51-414} in a mixed solvent of 6 M Gn-HCl, 200 mM Na_2HPO_4, and 2% Triton X-100 containing 150 mM 4-mercaptophenylacetic acid (MPAA) and 300 mM tris(2-carboxyethyl) phosphine hydrochloride (TCEP-HCl) at pH 7.0. As a result, the ligated product 6His-ENLYFQG-TDP_{1-414}(pS48) was obtained, albeit in low yield (Fig. 2a). Considering that the native chemical ligation between TDP_{39-49}(pS48)-thioester and Cys-TDP_{51-80} proceeded smoothly (see below for the synthesis of TDP_{1-80}), the low ligation yield to give full-length TDP-43 may be attributed to the high aggregation-prone property of LCD involved in TDP_{50-414}. Although the content of the ligated product, 6His-ENLYFQG-TDP_{1-414}(pS48) relative to Cys-TDP_{51-414} was low, the second half of the scheme with His-tag affinity chromatography allowed efficient separation of the ligated product from the remaining Cys-TDP_{51-414} (Fig. 2b). When the ligation mixture was applied to the nickel-nitrilotriacetic acid (Ni-NTA) column, the desired 6His-ENLYFQG-TDP_{1-414}(pS48) was supported on the stationary column, while unreacted Cys-TDP_{51-414} (without 6His-tag) was extracted in the fractions of flow-through (FT) and washing (W1). The ligated product was then eluted from the column by adding excess imidazole (E). The peptide linker connecting the 6His-tag and TDP_{1-414}(pS48) was subsequently cleaved by treatment with 6His-TEV protease, and the reaction mixture was passed through the second Ni-NTA column to extract the resulting G-TDP_{1-414}(pS48) in the FT and washing (W1) fractions (Fig. 2c). A combined fraction of FT and W1 was further applied to size exclusion chromatography (SEC) to remove the products derived from the unreacted TDP_{1-49}(pS48)-MeNbz, yielding G-TDP_{1-414}(pS48) as a pure form (Fig. 2d, e). Thus, the TDP_{1-414}(pS48) sample was obtained as a solution of 50 mM tris(hydroxymethyl)aminomethane (Tris)-HCl (pH 8.5), including 150 mM NaCl, 4% Triton X-100, and 1 mM dithiothreitol (DTT). We also synthesized non-phosphorylated TDP_{1-414} in the same manner (Fig. S6).

Self-association properties of full-length TDP-43

There was no detectable difference in the association state between TDP_{1-414}(pS48) and non-phosphorylated TDP_{1-414} on the synthesis. Thus, low-molecular-weight oligomers consisting of monomers to hexamers in similar abundance ratios were observed upon the final purification using SEC in the two species (protein concentrations: 8.0 μM each, Fig. S7). The initial association states after synthesis of TDP_{1-414}(pS48) and non-phosphorylated TDP_{1-414} are suggested by these results to be similar.

Next, we investigated the self-association tendency of TDP_{1-414}(pS48) and non-phosphorylated TDP_{1-414} at 37 °C (Figs. 3 and S8). First, the neutral pH buffer containing TDP_{1-414}(pS48) and unmodified TDP_{1-414} were incubated at 37 °C, and after certain periods of time (0, 6, 12, 24, 48, 72 h), the amounts of respective proteins in the supernatants following the centrifugation were quantified by SDS-PAGE (Figs. 3a and S9). In the sedimentation assay, the amounts of proteins in the supernatants decrease depending on the progress of the self-associations[22]. TDP_{1-414}(pS48) showed significantly higher protein contents in the supernatant at 6–48 h incubation times than those of unmodified TDP_{1-414}. TDP_{1-414}(pS48) is thus suggested to be less prone to self-association than unmodified TDP_{1-414}. Wang et al. reported that TDP_{1-414}(S48E), in which Ser48 was replaced with Glu, had a lower self-association tendency than the original TDP_{1-414}[3]. The present result using authentic TDP_{1-414}(pS48) is consistent with this report, in which the introduction of an anionic structure at position 48 suppresses the self-association of TDP_{1-414}. In addition, morphological analysis of TDP_{1-414}(pS48) and non-phosphorylated TDP_{1-414} was performed using transmission electron microscopy (TEM; Figs. 3b and S10). As previously reported[23], after incubation for a sufficient period of time (24 h), robust amyloid fibrils (x 15k) and oligomers of various sizes (x 30k) could be clearly observed in non-phosphorylated TDP_{1-414} (Fig. 3b). Interestingly, the situation was quite different in TDP_{1-414}(pS48), where typical amyloid fibrils were not observed. Instead, many large aggregates with diameters exceeding 100 nm were observed (Figs. 3b and S10). The results using TEM suggest significant differences in the final aggregate morphology of TDP_{1-414}(pS48) and non-phosphorylated TDP_{1-414}.

Studies on N-terminal TDP_{1-80}

Intermolecular associations between NTDs reportedly make an important contribution to forming the physiological self-assembly of TDP-43 in the nucleus[3,15,24,25]. It is therefore thought to be possible that the attenuated self-association of TDP_{1-414}(pS48) rather than unmodified TDP_{1-414} is attributed to the electrostatic repulsion between NTDs due to the phosphate anion at Ser48. To investigate the impact of phosphorylation on the association between NTDs, we subsequently performed the studies using the NTD, that is, TDP_{1-80}. TDP_{1-80}(pS48) and non-phosphorylated TDP_{1-80} were therefore synthesized by sequential native chemical ligations (Fig. S12). First, we confirmed that the secondary structure of the chemically synthesized non-phosphorylated TDP_{1-80} was consistent with that of the recombinantly prepared TDP_{1-80} by measuring the circular dichroism spectrum (Fig. S13). This result indicates that although the TDP_{1-80} polypeptide was constructed via native chemical ligation in the denaturing conditions (a buffer containing 6 M Gn-HCl) in the chemical synthesis, TDP_{1-80} properly refolded when redissolved in a buffer after removing the denaturant (using HPLC). Then, the self-association propensity of TDP_{1-80}(pS48)

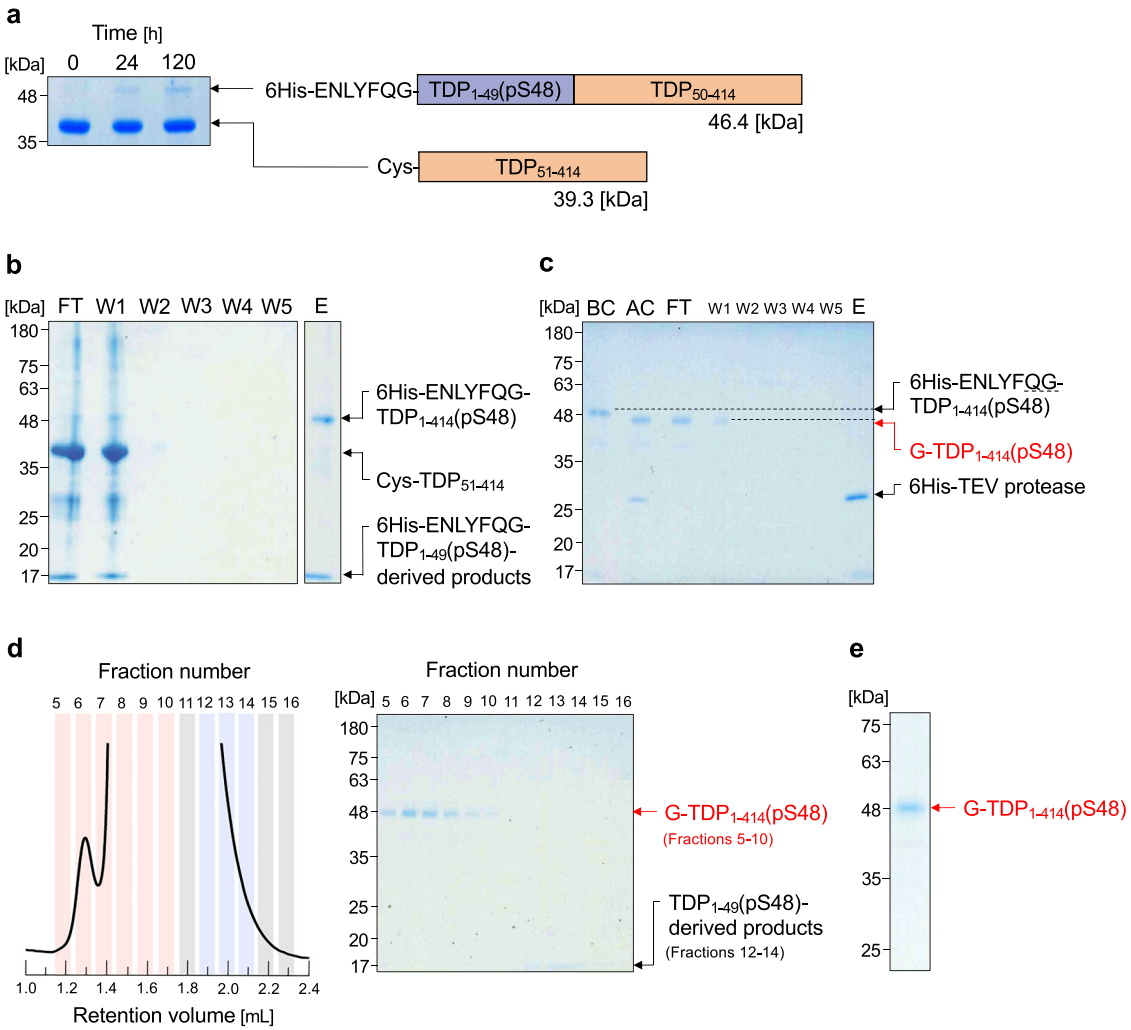

Fig. 2 | Semi-synthesis of TDP_{1-414}(pS48). a Sodium dodecylsulfate-polyacrylamide gel electrophoresis (SDS-PAGE) analysis on the native chemical ligation between 6His-ENLYFQG-TDP_{1-49}(pS48)-MeNbz-3Arg and Cys-TDP_{51-414}. The ligation reaction was performed at room temperature under the following conditions: 4 mM TDP_{1-49}(pS48)-MeNbz derivative, 0.4 mM Cys-TDP_{51-414}, 150 mM MPAA, 300 mM TCEP-HCl, 6 M Gn-HCl, 200 mM Na_2HPO_4, 2% Triton X-100 (pH 7.0). **b** 1st 6His-tag affinity chromatography. SDS-PAGE analysis of flow-through (FT), washing (W1–W5), and elution (E) fractions is shown. **c** Treatment with TEV protease followed by 2nd 6His-tag affinity chromatography. SDS-PAGE of before cleavage (BC), after cleavage (AC), flow-through (FT), washing (W1–W5), and elution (E) fractions are shown. The cleavage reaction was performed at 4 °C for 72 h under the following conditions: 50 mM Tris-HCl (pH 8.5), 2% Triton X-100, 1 mM DTT, 300 units 6His-TEV protease. **d** SEC of the combined fraction of FT and W1 in (**c**) (left part). The SEC analysis was performed with Superdex 75 5/150 GL at room temperature under the following conditions: an isocratic elution with 50 mM Tris-HCl (pH 8.5) including 150 mM NaCl, 0.1% Triton X-100, and 1 mM DTT, 0.3 mL/min. The contents of the SEC fractions were analyzed by SDS-PAGE due to overlapping UV absorption with Triton X-100 on the SEC chromatogram. The fractions 5–10 containing TDP_{1-414}(pS48), colored in light red, were separated from fractions 12–14 containing the products derived from TDP_{1-49}(pS48)-MeNbz derivative, colored in light blue. **e** The final pure sample of TDP_{1-414}(pS48) (combined fraction of #5–10 in **d**).

and non-phosphorylated TDP_{1-80} in the neutral pH buffer was verified using SEC (Fig. 4a). As a result, TDP_{1-80}(pS48) gave the assemblies with lower molecular weight, judging from the elution peak at larger retention volumes than the unmodified TDP_{1-80}. The lower association tendency of TDP_{1-80}(pS48) relative to the unmodified TDP_{1-80} was observed at the protein concentrations of 1 mM and 200 μM, and the difference between the two was barely discernible when the concentration was reduced to 40 μM. The lower self-association of TDP_{1-80}(pS48) than the unmodified TDP_{1-80} was also supported by crosslinking experiments using amine-reactive linker BS3, in which two *N*-hydroxysuccinimide active esters are present (molar ratio of protein:BS3 = 1:50) (Fig. S14)[3]. Regarding the detection using SDS-PAGE, the relative intensity of the bands derived from intermolecularly crosslinked products versus monomer was smaller in TDP_{1-80}(pS48) than that in the unmodified TDP_{1-80}. The crosslinked products with larger molecular weights were observed in both TDP_{1-80}(pS48) and the unmodified TDP_{1-80} as the protein concentration for the crosslinking reaction increased (40, 120, and 200 μM). However, consistency across all concentrations was that the phosphorylated form gave fewer crosslinked products than the unmodified form. Wang et al. reported from SEC and crosslinking experiments that a phosphoserine mimic in which Ser48 in TDP_{1-80} was replaced by Glu (i.e., TDP_{1-80}[S48E]) exhibited reduced self-association compared with intact TDP_{1-80}[3]. Our results, therefore, show that the authentic Ser48 phosphorylated form attenuates the self-association between NTDs, similar to TDP_{1-80}(S48E) (a comparison experiment between TDP_{1-80}[pS48] and TDP_{1-80}[S48E] is shown in Fig. S15).

To gain insight into the structural basis for the lower propensity in the self-association of TDP_{1-80}(pS48) than the unmodified TDP_{1-80}, we analyzed the differences in three-dimensional structures of the two species. We hypothesized that the solution structure of TDP_{1-80}(pS48) could be solved using small-angle X-ray scattering coupled with SEC (SEC-SAXS). Namely, the sharp and symmetrical major peak of TDP_{1-80}(pS48) on the SEC analysis (Fig. 4a, top of approximately 1.9 mL of retention volume; see also

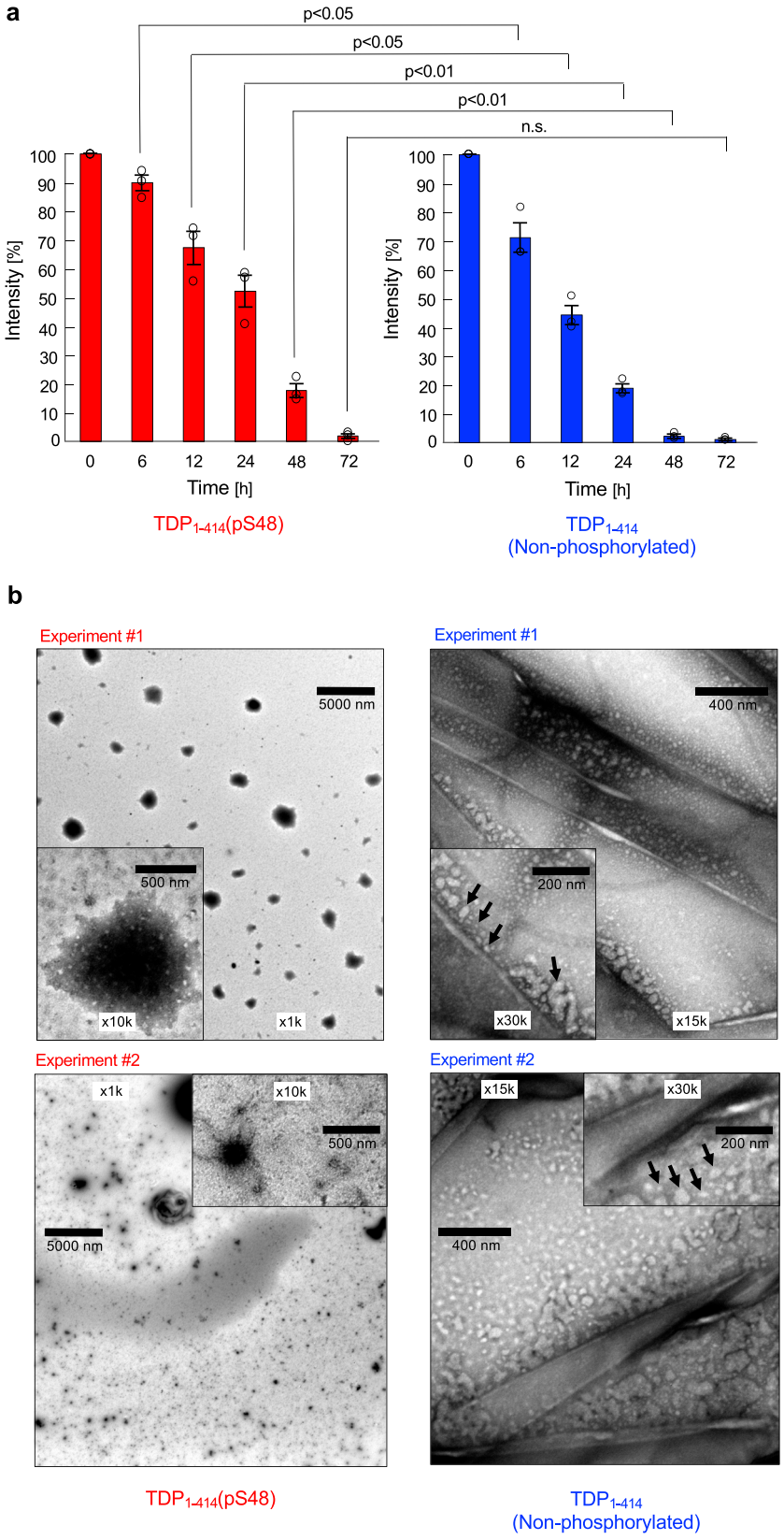

Fig. 3 | Self-association of $TDP_{1\text{-}414}$(pS48) and non-phosphorylated $TDP_{1\text{-}414}$ in the neutral pH buffer at 37 °C. a Sedimentation assay. The relative band intensities on the SDS-PAGE analysis of the supernatants after incubating the samples at 37 °C for certain periods of time (0, 6, 12, 24, 48, 72 h) are shown. The relative intensity values from the three independent experiments are plotted (open circles), and the mean ± SEM is overlaid. The *p*-values of Student's *t*-test between $TDP_{1\text{-}414}$(pS48) and non-phosphorylated $TDP_{1\text{-}414}$ are indicated. **b** TEM analysis. Micrographs of $TDP_{1\text{-}414}$(pS48) and non-phosphorylated $TDP_{1\text{-}414}$ after 24 h of incubation at 37 °C are shown. In the inset of non-phosphorylated $TDP_{1\text{-}414}$, the arrows point to the oligomers of various sizes. A micrograph of buffer only (no protein) was also analyzed as a control (Fig. S11). Micrographs from the two independent experiments are shown for both $TDP_{1\text{-}414}$(pS48) (left two images from experiment #1 and #2) and non-phosphorylated $TDP_{1\text{-}414}$ (right two images from experiment #1 and #2).

Figs. S16 and S17a) suggested the existence of a homogeneous association state, suitable for SAXS analysis. Prior to the analysis with SEC-SAXS, we measured the absolute molecular weight of the SEC peaks of $TDP_{1\text{-}80}$(pS48) using a multi-angle light scattering coupled with SEC (SEC-MALS) (Fig. S16). $TDP_{1\text{-}80}$(pS48) was shown to give a major peak with a molecular weight of 8.8×10^3 (± 2.0%), corresponding to the monomer. We thus collected SAXS data from the major peak on SEC analysis for solving the solution structure of $TDP_{1\text{-}80}$(pS48) as a monomer (Fig. S17).

The X-ray scattering profile obtained by the SEC-SAXS experiment provided an ab initio bead model representing the molecular geometry of

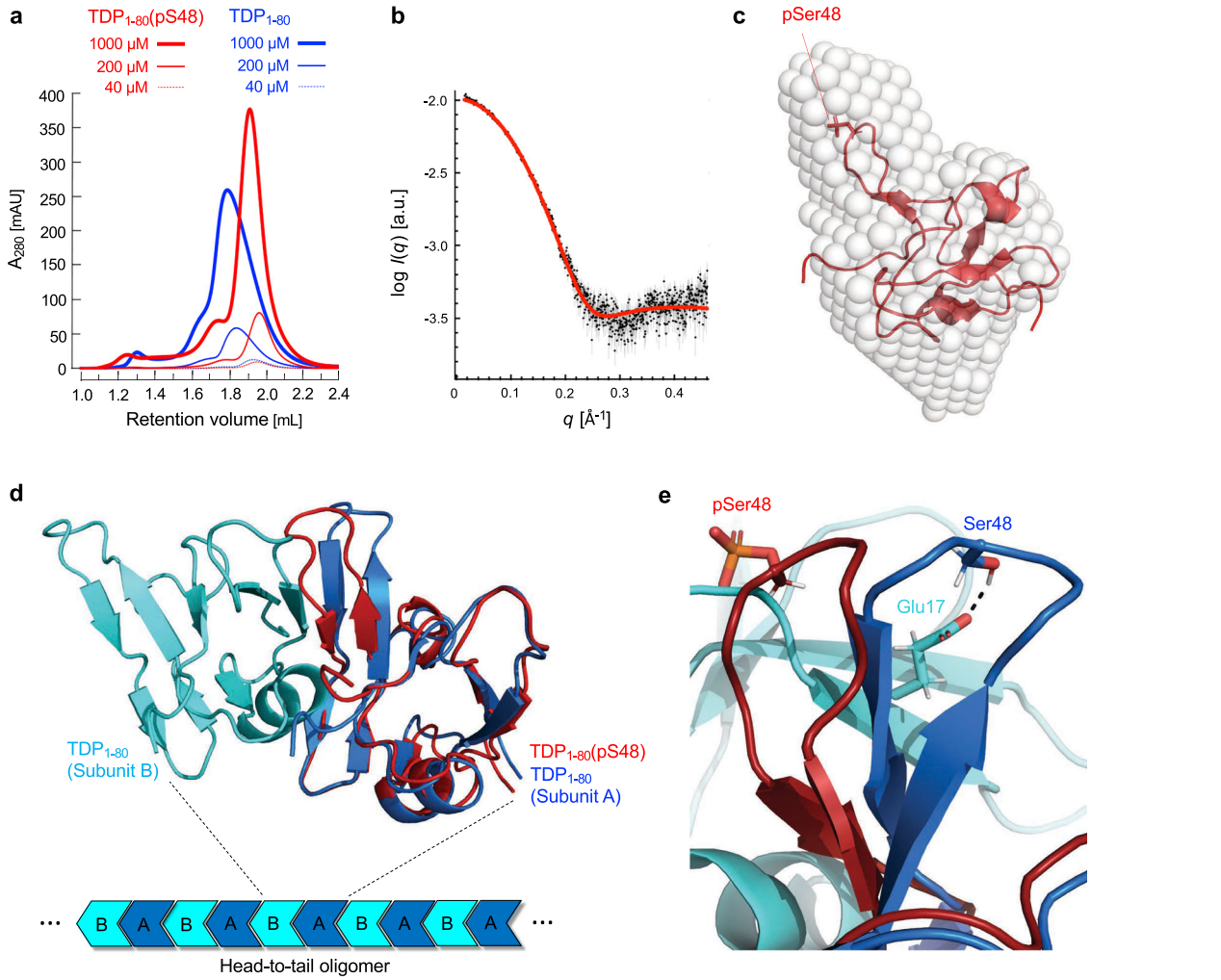

Fig. 4 | Solution structure analysis of $TDP_{1\text{-}80}$(pS48). a SEC of $TDP_{1\text{-}80}$(pS48) and unmodified $TDP_{1\text{-}80}$ at varied concentrations. SEC analysis was performed with Superdex 75 5/150 GL at room temperature under the following conditions: an isocratic elution with 50 mM Tris-HCl (pH 8.5) including 150 mM NaCl and 1 mM DTT, 0.3 mL/min. **b** X-ray scattering profiles obtained by the SEC-SAXS experiment (see also Fig. S17). Log scale scattering intensities (log $I(q)$) vs. vectors (q) are plotted in black dots. The scattering profile calculated for the determined three-dimensional structure of $TDP_{1\text{-}80}$(pS48) in (**c**) is shown as a red line. The calculated profile is in good agreement with the original SAXS data ($\chi^2 = 1.62$), supporting the validity of the determined structure of $TDP_{1\text{-}80}$(pS48). **c** Ab initio bead model (white sphere) and determined three-dimensional structure of $TDP_{1\text{-}80}$(pS48) (red cartoon). **d** The NMR structure of non-phosphorylated $TDP_{1\text{-}80}$ dimer unit, in which the two subunits interact in the head-to-tail fashion (PDB ID: 6B1G)[3], and superimposition of the determined structure of $TDP_{1\text{-}80}$(pS48) on one protomer (Subunit A). **e** Close-up view of the β-strand-loop-β-strand regions including Ser48 in $TDP_{1\text{-}80}$(pS48) (red cartoon) and non-phosphorylated $TDP_{1\text{-}80}$ (blue cartoon) to compare the structures at the inter-NTD interface. The hydrogen bond between the side chains of Ser48 (Subunit A) and Glu17 (Subunit B) is shown by the dotted line.

$TDP_{1\text{-}80}$(pS48) monomer (Fig. 4b, c). Then, on the basis of the atomic coordinates of a protomer of non-phosphorylated $TDP_{1\text{-}80}$ extracted from the solution NMR structure of $TDP_{1\text{-}80}$ dimer (PDB ID: 6B1G)[3], we successfully determined the three-dimensional structure of $TDP_{1\text{-}80}$(pS48) monomer (Figs. 4c and S17f). The scattering profiles calculated for the determined three-dimensional structure of $TDP_{1\text{-}80}$(pS48) showed high fidelity to the original SAXS data (Fig. 4b), supporting the validity of the determined structure of $TDP_{1\text{-}80}$(pS48). Interestingly, striking structural differences between $TDP_{1\text{-}80}$(pS48) and unmodified $TDP_{1\text{-}80}$ were observed in the β-strand-loop-β-strand region, including Ser48, whereas the remainder of the two structures was almost identical (Fig. S17g). In the reported dimer unit of non-phosphorylated $TDP_{1\text{-}80}$, the side chain hydroxy group of Ser48 (–OH) forms a hydrogen bond with the side chain carboxylate of Glu17 ($–COO^-$) intermolecularly, which makes the inter-NTD interaction in a head-to-tail fashion (Fig. 4d, e)[3,15,26]. On the other hand, a structural comparison, in which $TDP_{1\text{-}80}$(pS48) was superimposed on the $TDP_{1\text{-}80}$ protomer (Subunit A) in the dimer unit, showed that the side chain of phosphorylated Ser48 is located outside the range that intermolecularly forms the hydrogen bond with the side chain of Glu17. Similar results were obtained when $TDP_{1\text{-}80}$(pS48) was superimposed on the X-ray crystal structure of non-phosphorylated $TDP_{1\text{-}80}$[15] (Fig. S18). The electrostatic repulsion between the side chains of phosphorylated Ser48 ($–OPO_3^{2-}$) and Glu17 ($–COO^-$) might possibly induce the β-strand-loop-β-strand around Ser48 to form such a geometry and cause $TDP_{1\text{-}80}$(pS48) to have a lower self-association property compared with non-phosphorylated $TDP_{1\text{-}80}$.

Conclusions

$TDP_{1\text{-}414}$(pS48), a full-length TDP-43 possessing post-translational phosphorylation at Ser48, was semi-synthesized by native chemical ligation of $TDP_{1\text{-}49}$(pS48)-thioester surrogate and Cys-$TDP_{51\text{–}414}$. Affinity chromatography using His-tag, which was introduced into the $TDP_{1\text{-}49}$ side, was key to achieving the ligation product with high purity. Interestingly, $TDP_{1\text{-}414}$(pS48), unlike non-phosphorylated TDP-43, was found to have weak self-association properties and to form aggregates that were not typical amyloid fibrils under the physiological conditions (neutral pH and 37 °C). Furthermore, chemical synthesis and three-dimensional structure analysis

of the NTD fragment (TDP_{1-80}) suggested that the phosphate ion at the side chain of Ser48 attenuated the inter-NTD interaction by inducing electrostatic repulsion. TDP-43 is physiologically associated via interaction between the NTDs in the nucleus[3,15,24,25]. However, attenuating the interaction between the NTDs results in dissociation of TDP-43, which disrupts the RNA metabolism[3]. In addition, unassociated TDP-43, exported to the cytoplasm, becomes more susceptible to proteolytic cleavage than the associated TDP-43, resulting in the elevated release of the LCD fragments, which accelerates the amyloid aggregation[15]. According to the mechanism, it is conceivable that TDP_{1-414}(pS48) exacerbates ALS by attenuating the interaction between NTDs, which disrupts RNA metabolism in the nucleus and promotes amyloid formation in the cytoplasm. We are currently conducting studies concerning the plausible pathological mechanisms of TDP_{1-414}(pS48). At the same time, following our successful chemical synthesis of full-length TDP-43, the syntheses of other post-translationally modified forms of TDP-43[27,28] are ongoing. These comprehensive studies, which are based on the present outcome, will shed light on the currently elusive involvement of post-translational modifications of TDP-43 in the neurodegenerative diseases.

Methods

Recombinant expression of TDP_{50-414}

The plasmid pTDP_{50-414}, where the TDP_{50-414} gene with CBD and *Ssp* DnaB intein (Intein) genes at its N-terminus is cloned into the pTWIN1 vector (New England Biolabs Inc., Ipswich, MA), was designed (Fig. S19, plasmid map drawing was prepared with SnapGene [GSLBiotech LLC, Boston, MA] [www.snapgene.com]) and purchased from GenScript (Piscataway, NJ). T7 Express Competent *E. coli* host strain cells (New England Biolabs Inc., Ipswich, MA) were transformed with the plasmid and grown on Luria-Bertani (LB) agar medium supplemented with 100 μg/mL ampicillin. The resultant single colony was grown in LB broth medium supplemented with 100 μg/mL ampicillin at 37 °C for 16 h with shaking at 200 rpm. 10 mL of the culture was inoculated into 1 L of LB broth medium supplemented with 100 μg/mL ampicillin and grown at 37 °C with shaking at 200 rpm until the optimal density of 600 nm reached 0.4. The culture was incubated at 18 °C for 1 h, and isopropyl β-D-thiogalactopyranoside was added. Overexpression was induced at 18 °C for 16 h with shaking at 200 rpm, and the cells were harvested by centrifugation (13,260 × *g*, 4 °C, 15 min) and washed with phosphate-buffered saline (pH 7.4). The cells were then harvested by centrifugation (2380 × *g*, 4 °C, 15 min), frozen in liquid nitrogen, and stored at −80 °C until use.

The cells were thawed on ice, suspended in a lysis buffer (20 mM Tris-HCl [pH 8.5], 500 mM NaCl, 1 mM ethylenediamine-*N*,*N*,*N*′,*N*′-tetraacetic acid [EDTA], 2% Triton X-100, 1 mM DTT) containing 20 μM phenylmethylsulfonyl fluoride as a protease inhibitor, and disrupted by sonication on ice. The cell debris was collected by centrifugation (21,610 × *g*, 4 °C, 60 min), frozen in liquid nitrogen, and stored at −80 °C until use. The cell debris was suspended in solubilization buffer of 4 M Gn-HCl, 20 mM Tris-HCl (pH 8.5), 500 mM NaCl, 1 mM EDTA, 2% Triton X-100, and 1 mM DTT and incubated with agitation at 4 °C for 1 h to solubilize CBD-Intein-TDP_{50-414}. The cell debris was removed by centrifugation (33,770 × *g*, 4 °C, 60 min), and the supernatant was filtered with 0.45 μm filter and then dialyzed against the buffer of 20 mM Tris-HCl (pH 8.5), 500 mM NaCl, 1 mM EDTA, 2% Triton X-100, and 1 mM DTT at 4 °C for 24 h. The dialyzed protein solution was filtered with 0.45 μm filter and applied to a chitin resin (New England Biolabs Inc., Ipswich, MA)-packed CBD affinity column equilibrated with a buffer of 20 mM Tris-HCl (pH 8.5), 500 mM NaCl, 1 mM EDTA, 2% Triton X-100, and 1 mM DTT. The resin was washed with a buffer of 20 mM Tris-HCl (pH 8.5), 500 mM NaCl, 1 mM EDTA, 2% Triton X-100, and 1 mM DTT to remove unbound proteins. The column was then flushed with a buffer containing 20 mM Tris-HCl (pH 6.5), 500 mM NaCl, 1 mM EDTA, 2% Triton X-100, and 1 mM DTT to shift the pH from 8.5 to 6.5, inducing on-column self-cleavage by Intein. After 1 week of incubation, the target TDP_{50-414} was eluted from the column and precipitated with a chloroform-methanol mixture. The resulting pellet was dried at room temperature and stored at 4 °C until use. Purity of the protein was confirmed by SDS-PAGE analysis (Fig. S2e). All CBD affinity chromatography steps were performed at 4 °C.

Primary sequence of CBD-Intein-TDP_{50-414} (Underlined is TDP_{50-414}) is as follows:

MKIEEGKLTNPGVSAWQVNTAYTAGQLVTYNGKTYKCLQPH
TSLAGWEPSNVPALWQLQNNGNNGLELRESGAISGDSLISLASTGK
RVSIKDLLDEKDFEIWAINEQTMKLESAKVSRVFCTGKKLVYILKTR
LGRTIKATANHRFLTIDGWKRLDELSLKEHIALPRKLESSSLQLSPE
IEKLSQSDIYWDSIVSITETGVEEVFDLTVPGPHNFVANDIIVHN
CMRGVRLVEGILHAPDAGWGNLVYVVNYPKDNKRKMDETDAS
SAVKVKRAVQKTSDLIVLGLPWKTTEQDLKEYFSTFGEVLMVQV
KKDLKTGHSKGFGFVRFTEYETQVKVMSQRHMDGRWCDCKLPN-
SKQSQDEPLRSRKVFVGRCTEDMTEDELREFFSQYGDVMDVFIPKP-
FRAFAFVTFADDQIAQSLCGEDLIIKGISVHISNAEPKHNSNRQ
LERSGRFGGNPGGFGNQGGFGNSRGGGAGLGNNQGSNMGGGM
NFGAFSINPAMMAAAQAALQSSWGMMGMLASQQNQSGPSGNN
QNQGNMQREPNQAFGSGNNSYSGSNSGAAIGWGSASNAGSGS
GFNGGFGSSMDSKSSGWGM

Native chemical ligation followed by His-tag affinity chromatography

Native chemical ligation to give 6His-ENLYFQG-TDP_{1-414}(pS48) was performed by dissolving TDP_{50-414} (0.4 mM) and 6His-ENLYFQG-TDP_{1-49}(pS48)-MeNbz-3Arg (4 mM) in a buffer of 6 M Gn-HCl, 200 mM Na_2HPO_4 (pH 7.0), 150 mM MPAA, 300 mM TCEP-HCl, and 2% Triton X-100 and then leaving the solution at room temperature for 5 days. The reaction mixture was diluted 20-fold with a buffer of 6 M Gn-HCl, 200 mM Na_2HPO_4 (pH 8.5), 20 mM TCEP-HCl, 2% Triton X-100, and 10 mM imidazole, and applied to a Ni-NTA agarose resin-packed His-tag affinity column equilibrated with a buffer of 6 M Gn-HCl, 200 mM Na_2HPO_4 (pH 8.5), 20 mM TCEP-HCl, 2% Triton X-100, and 10 mM imidazole, and incubated at 4 °C for 1 h (1st 6His-tag affinity chromatography). The resin was washed with a buffer of 6 M Gn-HCl, 200 mM Na_2HPO_4 (pH 8.5), 20 mM TCEP-HCl, 2% Triton X-100, and 10 mM imidazole to remove unbound proteins. 6His-ENLYFQG-TDP_{1-414}(pS48) was eluted from the column with a buffer of 6 M Gn-HCl, 200 mM Na_2HPO_4 (pH 8.5), 20 mM TCEP-HCl, 2% Triton X-100, and 500 mM imidazole. The elution solution was exchanged into a buffer containing 50 mM Tris-HCl (pH 8.5), 2% Triton X-100, and 1 mM DTT, to which 6His-TEV protease (300 units) was added to induce cleavage of 6His-ENLYFQ. The reaction mixture was incubated at 4 °C for 3 days and then applied to a Ni-NTA agarose resin-packed His-tag affinity column equilibrated with buffer containing 50 mM Tris-HCl (pH 8.5), 2% Triton X-100, 1 mM DTT, and 10 mM imidazole, and G-TDP_{1-414}(pS48) was extracted in the flow-through fraction (2nd 6His-tag affinity chromatography). The resin was washed with buffer of 50 mM Tris-HCl (pH 8.5), 2% Triton X-100, 1 mM DTT, and 10 mM imidazole to give G-TDP_{1-414}(pS48) in the washing fraction. The column was treated with a buffer of 50 mM Tris-HCl (pH 8.5), 2% Triton X-100, 1 mM DTT, and 1 M imidazole to elute 6His-ENLYFQ and 6His-TEV protease, and recycled. The flow-through fraction and washing fraction were combined and precipitated with a chloroform-methanol mixture. The resulting pellet was then dissolved in a buffer of 50 mM Tris-HCl (pH 8.5), 150 mM NaCl, 0.1% Triton X-100, and 1 mM DTT (protein concentration: 8.0 μM, determined using a colorimetric method with Pierce™ 660_{nm} Protein Assay reagent [Thermo Scientific Inc., Waltham, MA]), and applied to SEC with a Superdex 75 5/150 GL column (GE Healthcare Technologies Inc., Chicago, IL) with an eluent of 50 mM Tris-HCl (pH 8.5), 150 mM NaCl, 0.1% Triton X-100, and 1 mM DTT at a flow rate of 0.3 mL/min to remove residual G-TDP_{1-49}(pS48) derivatives. The elution fractions were collected and analyzed by SDS-PAGE. SDS-PAGE band intensities on gels were quantified by ImageJ[29]. The desired elution fractions of G-TDP_{1-414}(pS48) were combined and filtered (concentrated) with an Amicon® Ultra 30 kDa MWCO centrifugal filter (Merck Millipore Ltd., Darmstadt, Germany). The resultant protein solution of

50 mM Tris-HCl (pH 8.5), 150 mM NaCl, 4% Triton X-100, and 1 mM DTT was stored at −80 °C until use. Final purity of the protein was confirmed by SDS-PAGE analysis (Fig. 2e), and the concentration was determined by Pierce™ 660 $_{nm}$ Protein Assay reagent (Thermo Fisher Scientific Inc., Waltham, MA). All steps of the His-tag affinity chromatography and SEC were performed at room temperature, and samples, and buffers were kept chilled on ice until use. Non-phosphorylated G-TDP_{1-414} was synthesized in a similar manner to that of G-TDP_{1-414}(pS48).

Sedimentation assay for Fig. 3a

TDP_{1-414}(pS48) and unmodified TDP_{1-414} dissolved in the solutions of 50 mM Tris-HCl (pH 8.5), 150 mM NaCl, 3% Triton X-100, and 1 mM DTT (protein concentrations: 3.0 μM) were incubated at 37 °C for the desired time periods (0, 6, 12, 24, 48, 72 h). Aliquot samples were centrifuged (20,630 × *g*, 4 °C, 15 min) at each time point, and the soluble protein in the supernatant was analyzed by SDS-PAGE. The SDS-PAGE band intensity on the gel was quantified by ImageJ[29], and the soluble protein ratio (%) was calculated. Three independent replicates ($n = 3$) were performed.

Transmission electron microscopy (TEM) for Figs. 3b, S10, and S11

TDP_{1-414}(pS48) and unmodified TDP_{1-414} dissolved in the solutions of 50 mM Tris-HCl (pH 8.5), 150 mM NaCl, 3% Triton X-100, and 1 mM DTT (protein concentrations: 3.0 μM) were incubated at 37 °C for 24 h. Aliquot samples were applied on the hydrophilic carbon-supported 200-mesh copper grid (Nisshin EM Co. Ltd., Tokyo, Japan). Excess samples were removed with filter paper after 15 min, and the samples on the grid were washed with a drop of water. The samples on the grid were negatively stained with EM stainer (Nisshin EM Co. Ltd., Tokyo, Japan) twice for 15 min and then air-dried for 20 min. Micrographs were collected with an accelerating voltage of 80 kV at 1000-fold, 10,000-fold, 15,000-fold, and 30,000-fold magnifications. The particle size distribution in the TEM micrographs (Fig. S10) was analyzed by ImageJ[29]. To exclude particles derived from Triton X-100 micelles with a diameter size of approximately 10 nm (Fig. S11), quantification was performed for particles ≥20 nm.

SEC analysis for Fig. 4a

TDP_{1-80}(pS48) and unmodified TDP_{1-80} were dissolved in a buffer of 50 mM Tris-HCl (pH 8.5), 150 mM NaCl, and 1 mM DTT (protein concentrations: 40, 200, and 1000 μM), and applied to SEC with a Superdex 75 5/150 GL column (eluent: 50 mM Tris-HCl [pH 8.5], 150 mM NaCl, and 1 mM DTT, flow rate: 0.3 mL/min). All steps of SEC analysis were performed at room temperature, and samples, and buffers were kept chilled on ice until use.

SEC-SAXS for Figs. 4b–e and S17

A buffer solution of 50 mM Tris-HCl (pH 8.5), 150 mM NaCl, 1 mM DTT, and 3% glycerol containing TDP_{1-80}(pS48) (protein concentration: 1000 μM) was prepared and subjected to in-line SEC-SAXS experiments on the BL38B1 beam line at SPring-8 (Hyogo, Japan). 200 μL of the sample solution of TDP_{1-80}(pS48) was applied to SEC with a Superdex 75 Increase 10/300 GL column (eluent: 50 mM Tris-HCl [pH 8.5], 150 mM NaCl, 1 mM DTT, and 3% glycerol, 20 °C, flow rate: 0.3 mL/min). SEC was operated on a SHIMADZU HPLC system. The sample was eluted into a sample cell with a 0.02 mm-thick quartz glass window and 1 mm path length. X-ray scattering images were collected using a PILATUS3 S 2M detector (Dectris Ltd., Baden, Switzerland) with a sample-detector distance of 2390 mm. The X-ray wavelength, beam size, and flux were 1.00 Å, 0.7 × 0.3 mm^2, and 1.1×10^{11} photons/s, respectively. A total of 1600 frames were collected during the elution of a column volume of 24 mL with a data acquisition time of 3 s/frame. The 2D images were processed with the SAngler program[30] to obtain 1D scattering profiles. The UV–vis spectra of the samples in the cells were simultaneously recorded on a QEpro UV–vis spectrometer (Ocean Insight Inc., Orlando, FL). The SAXS data were analyzed using the MOLASS program[31] as follows: the magnitude range of the scattering vector q used in the analysis was $0.015 < q\ (=4\pi\sin\theta/\lambda) < 0.46$ $Å^{-1}$, where θ is the half scattering angle and λ is the wavelength of the X-rays. Data for 28 consecutive frames during the elution of TDP_{1-80}(pS48) monomer were extracted and adopted as the final data. Scattering profiles, Guinier plots, and Kratky plots were obtained using the PRIMUS program in the ATSAS program suite[32]. The pair distance distribution function $P(r)$ was calculated using the GNOM program in ATSAS[33]. Using the DAMMIF program in ATSAS[34], an ab initio bead model was obtained using a D_{max} value of 42.9 Å, with the experimental $P(r)$ curve smoothly approaching zero. To obtain the structure of TDP_{1-80}(pS48) monomer, conformational ensembles accounting for the SAXS data were generated with the NMATOR program in ATSAS[32] using an atomic coordinate of one protomer (TDP_{1-80}[Y4R]) extracted from the previously reported solution NMR structure of the TDP_{1-80} dimer unit (PDB ID: 6B1G)[3]. One of the ensembles that fit well both the ab initio bead model and the experimental data was selected as the best structure and then modified by the Coot application[35]. The final structure of the TDP_{1-80}(pS48) monomer was evaluated with the CRYSOL program in ATSAS[36]. Structure drawings were prepared with PyMOL (Schrödinger LLC, New York, NY).

Data availability

The SEC-SAXS data and solution structure of TDP_{1-80}(pS48) have been deposited in the Small-Angle Scattering Biological Data Bank (SASBDB) with an accession code of SASDV74. All other data, including experimental procedures and analytical data, are provided in the Article, Supplementary Information and from corresponding authors upon request. Source data of Fig. 3a are provided as Supplementary Data 1.

Received: 7 November 2024; Accepted: 11 April 2025;
Published online: 25 April 2025

References

1. Ou, S.-H., Wu, F., Harrich, D., García-Martínez, L. F. & Gaynor, R. B. Cloning and characterization of a novel cellular protein, TDP-43, that binds to human immunodeficiency virus type 1 TAR DNA sequence motifs. *J. Virol.* **69**, 3584–3596 (1995).
2. Buratti, E. & Baralle, F. E. Multiple roles of TDP-43 in gene expression, splicing regulation, and human disease. *Front. Biosci.* **13**, 867–878 (2008).
3. Wang, A. et al. A single N-terminal phosphomimic disrupts TDP-43 polymerization, phase separation, and RNA splicing. *EMBO J.* **37**, e97452 (2018).
4. Winton, M. J. et al. Disturbance of nuclear and cytoplasmic TAR DNA-binding protein (TDP-43) induces disease-like redistribution, sequestration, and aggregate formation. *J. Biol. Chem.* **283**, 13302–13309 (2008).
5. Neumann, M. et al. Ubiquitinated TDP-43 in frontotemporal lobar degeneration and amyotrophic lateral sclerosis. *Science* **314**, 130–133 (2006).
6. Johnson, B. S. et al. TDP-43 is intrinsically aggregation-prone, and amyotrophic lateral sclerosis-linked mutations accelerate aggregation and increase toxicity. *J. Biol. Chem.* **284**, 20329–20339 (2009).
7. Li, W. et al. Heat shock-induced phosphorylation of TAR DNA-binding protein 43 (TDP-43) by MAPK/ERK kinase regulates TDP-43 function. *J. Biol. Chem.* **292**, 5089–5100 (2017).
8. Wu, R. et al. Phosphorylation of trans-active response DNA-binding protein-of 43 kDa promotes its cytoplasmic aggregation and modulates its function in tau mRNA stability and exon 10 alternative splicing. *J. Neurochem.* **158**, 766–778 (2021).
9. Gruijs da Silva, L. A. et al. Disease-linked TDP-43 hyperphosphorylation suppresses TDP-43 condensation and aggregation. *EMBO J.* **41**, e108443 (2022).
10. Lee, S. et al. c-Abl regulates the pathological deposition of TDP-43 via tyrosine 43 phosphorylation. *Cells* **11**, 3972 (2022).

11. Kent, S. B. H. Total chemical synthesis of proteins. *Chem. Soc. Rev.* **38**, 338–351 (2009).
12. Moon, S. P., Balana, A. T. & Pratt, M. R. Consequences of post-translational modifications on amyloid proteins as revealed by protein semisynthesis. *Curr. Opin. Chem. Biol.* **64**, 76–89 (2021).
13. Li, Q.-Q. et al. Uncovering the pathological functions of Ser404 phosphorylation by semisynthesis of a phosphorylated TDP-43 prion-like domain. *Chem. Commun.* **56**, 5370–5373 (2020).
14. Zhou, X. et al. Mutations linked to neurological disease enhance self-association of low-complexity protein sequences. *Science* **377**, eabn5582 (2022).
15. Afroz, T. et al. Functional and dynamic polymerization of the ALS-linked protein TDP-43 antagonizes its pathologic aggregation. *Nat. Commun.* **8**, 45 (2017).
16. Dawson, P. E., Muir, T. W., Clark-Lewis, I. & Kent, S. B. H. Synthesis of proteins by native chemical ligation. *Science* **266**, 776–779 (1994).
17. Mathys, S. et al. Characterization of a self-splicing mini-intein and its conversion into autocatalytic N- and C-terminal cleavage elements: facile production of protein building blocks for protein ligation. *Gene* **231**, 1–13 (1999).
18. Li, Q., Babinchak, W. M. & Surewicz, W. K. Cryo-EM structure of amyloid fibrils formed by the entire low complexity domain of TDP-43. *Nat. Commun.* **12**, 1620 (2021).
19. Kuo, P.-H., Chiang, C.-H., Wang, Y.-T., Doudeva, L. G. & Yuan, H. S. The crystal structure of TDP-43 RRM1-DNA complex reveals the specific recognition for UG- and TG-rich nucleic acids. *Nucleic Acids Res.* **42**, 4712–4722 (2014).
20. Kuo, P.-H., Doudeva, L. G., Wang, Y.-T., Shen, C.-K. J. & Yuan, H. S. Structural insights into TDP-43 in nucleic-acid binding and domain interactions. *Nucleic Acids Res.* **37**, 1799–1808 (2009).
21. Blanco-Canosa, J. B., Nardone, B., Albericio, F. & Dawson, P. E. Chemical protein synthesis using a second-generation *N*-acylurea linker for the preparation of peptide-thioester precursors. *J. Am. Chem. Soc.* **137**, 7197–7209 (2015).
22. Yang, L. et al. Effective inhibition of TDP-43 aggregation by native state stabilization. *Angew. Chem. Int. Ed.* **63**, e202314587 (2024).
23. Kumar, S. T. et al. Seeding the aggregation of TDP-43 requires post-fibrillization proteolytic cleavage. *Nat. Neurosci.* **26**, 983–996 (2023).
24. Mompeán, M. et al. Point mutations in the N-terminal domain of transactive response DNA-binding protein 43 kDa (TDP-43) compromise its stability, dimerization, and functions. *J. Biol. Chem.* **292**, 11992–12006 (2017).
25. Jiang, L.-L. et al. The N-terminal dimerization is required for TDP-43 splicing activity. *Sci. Rep.* **7**, 6196 (2017).
26. Wright, G. S. A. et al. Purification and structural characterization of aggregation-prone human TDP-43 involved in neurodegenerative diseases. *iScience* **23**, 101159 (2020).
27. Cohen, T. J. et al. An acetylation switch controls TDP-43 function and aggregation propensity. *Nat. Commun.* **6**, 5845 (2015).
28. Hans, F., Eckert, M., von Zweydorf, F., Gloeckner, C. J. & Kahle, P. J. Identification and characterization of ubiquitinylation sites in TAR DNA-binding protein of 43 kDa (TDP-43). *J. Biol. Chem.* **293**, 16083–16099 (2018).
29. Schneider, C. A., Rasband, W. S. & Eliceiri, K. W. NIH Image to ImageJ: 25 years of image analysis. *Nat. Methods* **9**, 671–675 (2012).
30. Shimizu, N. et al. Software development for analysis of small-angle x-ray scattering data. *AIP Conf. Proc.* **1741**, 050017 (2016).
31. Yonezawa, K., Takahashi, M., Yatabe, K., Nagatani, Y. & Shimizu, N. MOLASS: software for automatic processing of matrix data obtained from small-angle X-ray scattering and UV-visible spectroscopy combined with size-exclusion chromatography. *Biophys. Physicobiol.* **20**, e200001 (2023).
32. Manalastas-Cantos, K. et al. ATSAS 3.0: expanded functionality and new tools for small-angle scattering data analysis. *J. Appl. Crystallogr.* **54**, 343–355 (2021).
33. Svergun, D. I. Determination of the regularization parameter in indirect-transform methods using perceptual criteria. *J. Appl. Crystallogr.* **25**, 495–503 (1992).
34. Franke, D. & Svergun, D. I. DAMMIF, a program for rapid ab-initio shape determination in small-angle scattering. *J. Appl. Crystallogr.* **42**, 342–346 (2009).
35. Emsley, P., Lohkamp, B., Scott, W. G. & Cowtan, K. Features and development of Coot. *Acta Crystallogr. D. Biol. Crystallogr.* **66**, 486–501 (2010).
36. Franke, D. et al. ATSAS 2.8: a comprehensive data analysis suite for small-angle scattering from macromolecular solutions. *J. Appl. Crystallogr.* **50**, 1212–1225 (2017).

Acknowledgements

This research was supported by JSPS KAKENHI grant numbers JP21H02602 (Y.S.), JP24K02153 (Y.S.), JP24H01787 ("Latent Chemical Space", Y.S.), and JP24K09344 (D.S.). This research was also supported by Chugai Foundation for Innovative Drug Discovery Science (Y.S.), Astellas Foundation for Research on Metabolic Disorders (Y.S.), the Hoansha Foundation (Y.S.), the Takeda Science Foundation (Y.S.), and the 2022 Wakayama Medical Award for Young Researchers (D.S.). The part of the synchrotron radiation experiment in this study was supported by the Research Support Project for Life Science and Drug Discovery (Basis for Supporting Innovative Drug Discovery and Life Science Research (BINDS)) from AMED under Grant Number JP23ama121001. The part of the circular dichroism spectrum measurement and data analysis in this study were performed at the Analytical Instrument Facility, Graduate School of Science, Osaka University, which was supported by using research equipment shared in MEXT Project for promoting public utilization of advanced research infrastructure (Program for supporting construction of core facilities) grant number JPMXS0441200025. We thank Dr. Toru Nakatsu, Dr. Katsumasa Irie, and Dr. Satoru Tamura (Wakayama Medical University) for allowing us access to their experimental facilities. We also acknowledge proofreading and editing by Benjamin Phillis at the Clinical Study Support Center at Wakayama Medical University.

Author contributions

D.S. and Y.S. designed the research; D.S. and M.T. performed the research; D.S., M.T., and Y.S. analyzed the data; and D.S. and Y.S. wrote the paper.

Competing interests

The authors declare no competing interests.

Additional information

Supplementary information The online version contains supplementary material available at https://doi.org/10.1038/s42004-025-01522-1.

Correspondence and requests for materials should be addressed to Daisuke Sasaki or Youhei Sohma.

Peer review information *Communications Chemistry* thanks Matthew Pratt and the other anonymous reviewers for their contribution to the peer review of this work. Peer review reports are available.